

# Extreme statistics, Gaussian statistics, and superdiffusion in global magnitude fluctuations in turbulence

R. Labbé\* and G. Bustamante

*Laboratorio de Turbulencia, Departamento de Física, Facultad de Ciencia,  
Universidad de Santiago de Chile, USACH. Casilla 307, Correo 2, Santiago, Chile*

(Dated: December 8, 2011)

Extreme value statistics, or extreme statistics for short, refers to the statistics that characterizes rare events of either unusually high or low intensity: climate disasters like floods following extremely intense rains are among the principal examples. Extreme statistics is also found in fluctuations of global magnitudes in systems in thermal equilibrium, as well as in systems far from equilibrium. A remarkable example in this last class is fluctuations of injected power in confined turbulence. Here we report results in a confined von Kármán swirling flow, produced by two counter-rotating stirrers, in which quantities derived from the same global magnitude—the rotation rate of the stirrers—can display both, extreme and Gaussian statistics. We find, on the one hand, that underlying the extreme statistics displayed by the global shear of the flow, there is a nearly Gaussian process resembling a white noise, corresponding to the action of the normal stresses exerted by the turbulent flow, integrated on the flow-driving surfaces of the stirrers. On the other hand, the magnitude displaying Gaussian statistics is the global rotation rate of the fluid, which happens to be a realization of a 1D superdiffusion where the variance of the angular increments  $\theta(t + \Delta t) - \theta(t)$  scales as  $\Delta t^{\mu/2}$ , while the power spectral density of the rotation rate follows a  $f^{-1/\sigma}$  scaling law. We found that the values of  $\mu$  and  $\sigma$  are very close to the number  $e$ , and the occurrence of the number  $1/e$  in a different, albeit well known problem in finance and probability theory—the so called secretary, marriage, best choice, or optimal stopping problem—, suggest that  $e$  could indeed have a role in these scaling laws.

PACS numbers: 47.27.-i, 42.32.-y, 74.40.Gh

## I. INTRODUCTION

Turbulence is a complex phenomenon: it is characterized by the interaction of structures in the flow velocity field distributed in ranges of space and time scales spanning several decades<sup>1</sup>. Thus, treating it analytically or by direct numerical computing remains a major challenge and performing experiments is, and possibly will last, a valuable research approach<sup>2</sup>. Since some 20 years to now, a number of experiments in confined turbulent flows were performed in the so-called von Kármán swirling flow setup, in which a cylindrical vessel encloses a fluid stirred by two rotating disks with vanes, each facing the other and located near the ends of the container. One of the goals of these experiments is to increase the knowledge on energy transfer dynamics through turbulent flows, from global scales to smallest ones, where the energy is finally dissipated as heat. It was found that at the energy injection scale, fluctuations of injected power are characterized by an extreme statistics: the probability density function (PDF) displays a non-Gaussian shape, strongly asymmetric with a stretched tail towards the low dissipation end<sup>3,4</sup>. The existence of similar PDFs in a variety of very dissimilar systems raised considerable interest in fluctuations of global magnitudes having PDFs with this particular shape<sup>5-7</sup>, linking together systems in thermal equilibrium with systems far from equilibrium, that is, those needing a permanent energy flow through them to stay in a statistically steady state. More recent works targeted the changes that under different condi-

tions can undergo the statistics of global magnitudes in these systems<sup>8-11</sup>. In a carefully controlled experiment in a confined von Kármán swirling flow, we found that extreme statistics, as well as Gaussian statistics, can be either displayed or hidden in global magnitudes derived from the same dynamical variables. On the one hand, underlying a magnitude displaying extreme statistics we found torque fluctuations with nearly Gaussian statistics, small auto-correlation time, and flat spectrum, suggesting that the torque resulting from the turbulent flow stresses acting on the surface of the stirring devices resembles a Gaussian white noise. On the other hand, we found that for a global magnitude having Gaussian statistics there is an underlying dynamics that behaves like a superdiffusion process with scaling laws where the number  $e$  seems to play a central role.

## II. DEFINITION, DYNAMICS AND MEASUREMENT OF GLOBAL MAGNITUDES

Here, our focus will be set on a counterrotating von Kármán swirling flow driven at constant torque, where one of the fluctuating magnitudes is the injected power

$$p = \Omega_1 \tau_1 + \Omega_2 \tau_2. \quad (1)$$

In equation (1)  $\Omega_1, \Omega_2$  are the angular speeds of the rotating stirrers that drive the flow, and  $\tau_1, \tau_2$  are the torques provided by electrical motors that keep them rotating. In (1) we assume that torques related to mechan-

ical and electrical losses are already discounted. Our experimental setup can be seen in Fig. 1. The turbulent flow is produced inside a cylindrical container by two low inertia stirrers driven by low inertia servomotors. These stirrers are located near the ends of the cylinder, and rotate in opposite directions. Details of the experimental setup are given in Appendix A. We made measurements at mean rotation rates of 16 revolutions per second (rps) and 32 rps. As usual, we define the Reynolds number for each stirrer as  $Re = \Omega^2 R / \nu$ , where  $R$  is the radius of the stirrers,  $\Omega$  is measured in  $\text{rad s}^{-1}$ , and  $\nu$  is the kinematic viscosity of air. Thus, at the previously mentioned rotating frequencies, and after correcting the kinematic viscosity for each equilibrium temperature, the Reynolds numbers are  $Re = 2.1 \times 10^5$  at  $32.5^\circ\text{C}$ , and  $Re = 3.4 \times 10^5$  at  $72^\circ\text{C}$ , respectively. In equation (1), all of the magnitudes could be functions of time, but the analysis becomes simpler when some of them are held constant. Here we have chosen to keep torques constant, the so-called  $\Gamma$  mode by Tiron and Cadot<sup>12</sup>. This choice allows a cleaner experiment: the risk of introducing artifacts because of controllers not optimally tuned, always present in experiments carried at constant velocity, is simply nonexistent. This also allows the stirrers to freely respond to changes in the flow reaction torque, contrarily to the case in which their rotation rate is held constant. Ideally, this last condition would correspond to the case of stirrers having infinite inertia: a limit that is practically impossible to achieve due to natural limitations of servo controllers. Instead, in the constant torque mode only good quality voltage-controlled current sources are needed, along with motors capable of delivering constant torque at constant current no matter their rotation rate. Both of these requirements are met by our experimental setup when operates under the conditions already specified.

Dimensional analysis tell us that the torque exerted by the turbulent flow on a rotating stirrer has the form  $\tau_F = \eta_F \Omega^2$ , where  $\eta_F = C_D \rho(P, T) R^5$ . Here,  $\rho$  is the density of the fluid, and is a function of the pressure  $P$  and the absolute temperature  $T$ ,  $R$  is the radius of the stirrer, and  $C_D$  is a dimensionless coefficient that can be determined experimentally. By writing all the dynamical variables as a sum of a mean value and a fluctuating part, we find that the stirrers' motion is governed by the following coupled Langevin equations:

$$J \frac{d\tilde{\Omega}_i}{dt} + (\gamma_M + 2\eta_F \bar{\Omega}) \tilde{\Omega}_i = \tilde{\tau}_i, \quad i = 1, 2, \quad (2)$$

where  $J$  is the moment of inertia of each stirrer (including motor armature and rotating coupling components), tildes specify the fluctuating part of magnitudes varying in time, while over bars indicate their time average. The mean value of the angular speed,  $\bar{\Omega}$ , is assumed identical for both stirrers, which implies a vanishing mean rotation rate for the global flow rotation. Thus, we can neglect in (2) the weak torque exerted by the cylinder wall, although it is that torque what allows for the global rota-

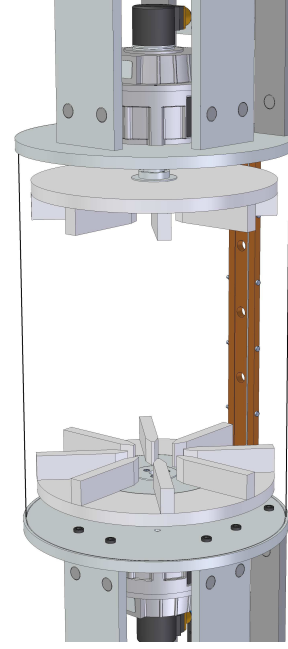


FIG. 1. Drawing of the experimental setup. Two low inertia stirrers are enclosed in a cylindrical vessel, each one driven by a low inertia servomotor (see text).

tion rate to have a definite mean value. The parameter  $\gamma_M$  is the viscous coefficient for electrical losses in the motors, and is given by the manufacturer. We ascribe the coupling between the stirrers fluctuating angular speeds  $\tilde{\Omega}_1$  and  $\tilde{\Omega}_2$  to the cross-correlation between the fluctuating torques  $\tilde{\tau}_1$  and  $\tilde{\tau}_2$ . The quantities  $\tilde{\Omega}_1$  and  $\tilde{\Omega}_2$  were obtained from the measurement of the angular speeds  $\Omega_1$  and  $\Omega_2$  by detrending the data using a quadratic polynomial. We did so because data trends related to slow changes in the air temperature during the measurement runs were not always linear.

Equations (2) imply that there exists a cutoff frequency  $\omega_c = 2\pi f_c$  for the fluctuations in the stirrers angular speed,

$$f_c = \frac{\gamma_M + 2\eta_F \bar{\Omega}}{2\pi J}, \quad (3)$$

which will be larger for faster mean rotation speeds, and can be further increased if the total moment of inertia of the stirrer is reduced. We cannot reduce to zero the inertia, but using equations (2) the measured angular speeds can be deconvolved to obtain the torque exerted by the turbulent flow on the stirrers —a surrogate of a zero-inertia measurement. Fig. 2 shows the power spectral density (PSD) for angular speeds fluctuations at 16 rps and 32 rps. We note that the flat horizontal regions, along with the roll-offs displaying a  $f^{-2}$  scaling past the first corner, are exactly the frequency responses associated to equations (2), suggesting that the spectrum of torque fluctuations is flat even beyond these first cutoff frequencies. The effect of the mean angular speed on the cutoff frequencies is evidenced by the shift to higher fre-

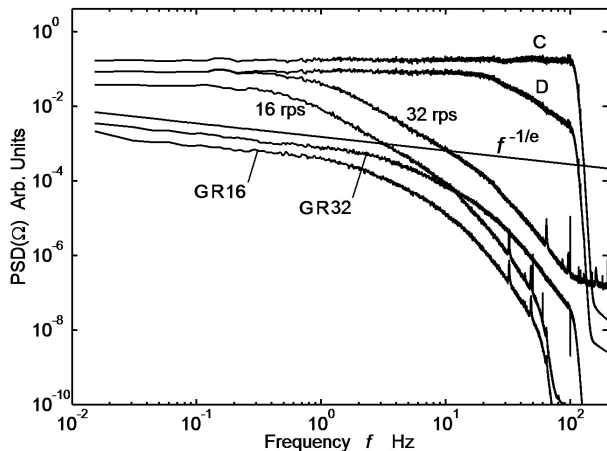


FIG. 2. Spectra of the angular speed  $\Omega$  of the lower disk. The curves labeled 16 rps and 32 rps correspond to the spectra of the lower stirrer rotating at those mean rates, respectively. The deconvolved spectrum (D) corresponds to the torque fluctuations obtained by deconvolution of the signal at 32 rps. The compensated spectrum (C), here raised by a factor two for clarity, is obtained when the surface averaging effect is removed from the time signal (see text). The global rotation spectra (GR) for 16 rps and 32 rps are represented by the two bottom curves. The straight line illustrates the scaling exponent of the spectra corresponding to 32 rps in the frequency region below  $\approx 2.6$  Hz. The lowest curve is the global rotation spectra for disks rotating at 16 rps. We see that in this last case the straight region is found below  $\approx 1$  Hz.

quencies in the roll-off of the spectrum when the rotation rate is increased from 16 rps to 32 rps. The ratio between those cutoff frequencies can be quantified by using equation (3), giving  $f_c^{(32)}/f_c^{(16)} = 1.763$ , whereas the ratio obtained from a fit of the frequency response of equations (2) to the measured spectra is  $f_c^{(32)}/f_c^{(16)} = 1.752$ . Note that the discrepancy is smaller than 0.7%, a remarkably good agreement suggesting that the approximation given by equations (2) adequately captures the global dynamics of the system.

### III. GLOBAL SHEAR STATISTICS

If we take the signal corresponding to 32 rps and deconvolve it in the Fourier space, we arrive to the torque fluctuations, whose spectrum is labeled (D) in Fig. 2. In this process, by using appropriate filters we also removed all the spurious peaks present in the primitive spectrum (see Appendix B). In this spectrum a second corner can be seen, also visible in the spectra labeled 16 rps and 32 rps, at roughly 10 Hz and 22 Hz, respectively. These secondary cutoff frequencies are not related to inertia effects. They can be ascribed instead to the averaging of normal stresses exerted by the flow on the vertical surfaces of the vanes. We note that this cutoff is similar to that seen in a previous experiment in which the ro-

tation speed was held constant<sup>3</sup>. There, inertia effects were highly reduced by the action of the servo controller, and the observed cutoff, incorrectly attributed only to inertia, was indeed the combination of an inertia cutoff shifted towards higher frequencies, with this second cutoff. This resulted in spectra displaying single corners, and single roll-offs regions for torque fluctuations with a  $1/f^4$  scaling beyond the cut-off frequency.

We can interpret the second cutoff as the results of the surface averaging of structures in the turbulent velocity field with sizes smaller than the characteristic size of a vane. Many of these structures are advected by the mean flow, and when encounter the vanes they originate normal stresses that push the surface at more or less random times on different locations. Of course, smaller sizes and larger separation in these flow structures mean less correlated actions on the surface. The final effect of this process is a decreasing energy in the power spectrum of  $\Omega$  with increasing frequency  $f$ , as higher frequencies are related to smaller structures in the flow. We can try to compensate for this effect as follows: inertia filtering is a sort of time average, one in which causality plays an important role. Only past events can enter in the average, and older events are forgotten with a weight factor that decreases with the elapsed time. This is related to the existence of a phase shift—which is a function of  $f$ —in the convolution of the time signal. By analogy with this process, we can attempt to remove the effect of space averaging from the time signal. The difference is that in this case there is no phase shift involved: the adding-up of signals is performed on the surface of the vanes. No causal relationship exists, at least in principle, between events occurring at different places on the surface of the vanes, although all this is finally reflected in the time signal. Thus, we made a ‘deconvolution’ process using a zero phase—non causal—time filter, designed to maintain a flat spectrum beyond the second cutoff corner. We cannot go beyond the 100 Hz limit that we have chosen, because the signal to noise ratio of our measurement at higher frequencies precludes it. As a result of the previously described procedures, we obtain a signal with a flat spectrum, spanning four decades of frequencies from about  $10^{-2}$  Hz to 100 Hz. In Fig. 2 this is displayed in the spectrum labeled (C), raised by a factor two to avoid the overlap with the other spectra.

The PDFs of rotation rate fluctuations are displayed in Fig. 3. The PDFs of fluctuations corresponding to the lower and upper stirrer are the narrower asymmetric curves. As we drive the stirrers at constant torque, from equation (1) we see that the instantaneous power injected into the flow is proportional to the sum  $\Omega_1(t) + \Omega_2(t)$ . The PDF of this magnitude is represented by the wider asymmetric curve, and given that the stirrers rotate in opposite directions, it corresponds to fluctuations in the global shear applied to the flow. The other global magnitude that we can derive from these angular speeds is the global rotation rate, given by the difference  $\Omega_1(t) - \Omega_2(t)$ . The PDF of this magnitude is displayed by the symmet-

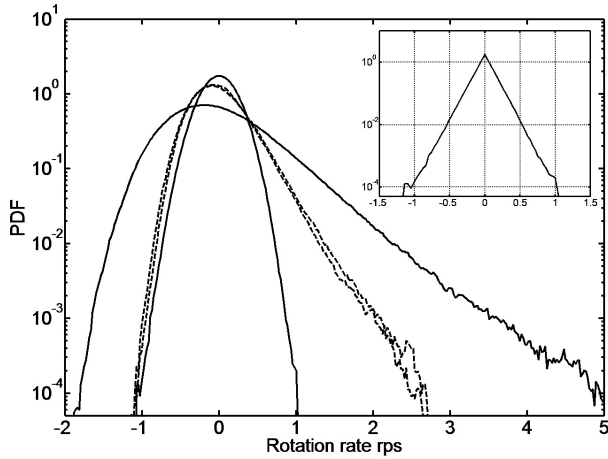


FIG. 3. Probability density functions. The asymmetric PDFs (dashed) correspond to fluctuations of the rotation rate in the lower and upper stirrers. The widest PDF corresponds to the sum  $\tilde{\Omega}_1(t) + \tilde{\Omega}_2(t)$ , which is proportional to fluctuations of the injected power. The narrow and symmetric PDF corresponds to the difference  $\tilde{\Omega}_1(t) - \tilde{\Omega}_2(t)$  which is related to the global rotation performed by the flow. The inset represents this last PDF, where the map  $x \mapsto x|x|$  was applied to the horizontal scale. This gives it an isosceles triangle-like shape, making evident its Gaussian character (see text).

ric curve, which happens to be *exactly* a Gaussian. To illustrate this, the inset is a representation using a logarithmic vertical scale, as usual, and the map  $x \mapsto x|x|$  on the horizontal scale. Using these transformations a Gaussian becomes the sides of an isosceles triangle, which is just what we see in the inset. Thus, we have here a somehow surprising finding: On the one hand, small departures from the state of zero mean rotation, related to the difference  $\tilde{\Omega}_1(t) - \tilde{\Omega}_2(t)$ , display a Gaussian statistics. On the other hand, the injected power related to the sum  $\tilde{\Omega}_1(t) + \tilde{\Omega}_2(t)$ , displays an extreme statistics, with a PDF stretched towards high angular speeds. We note here that this last behavior is consistent with the result reported in the work mentioned previously<sup>3</sup>: at constant speed, the injected power displays intense events towards the low power end, corresponding to low torque events signaling a weakening of the drag exerted by the flow on the stirrers. In the present case the external torque applied to the stirrers is constant; hence a sudden weakening in the drag torque implies a sudden increase in the angular speed, which is reflected here in a PDF of  $\tilde{\Omega}$  with a stretched right side.

Now we consider the effects on the PDFs of a) deconvolution; and b) compensation of surface averaging. The first procedure gives the PDF of torque fluctuations. The second one gives an estimate of torque fluctuations without surface averaging, in a range of scales corresponding to the frequency band from  $10^{-2}$  Hz to 100 Hz. In Fig. 4, the curve labeled (D) is the PDF of the torque. Note that the asymmetry is greatly reduced as compared to the PDF of the angular speed, but a stretching towards

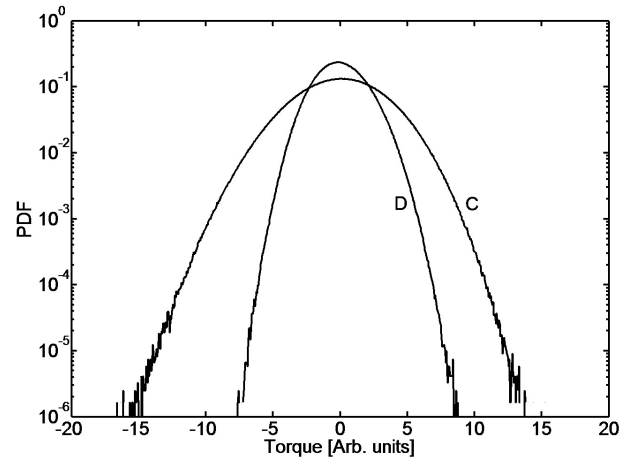


FIG. 4. Torque fluctuations PDFs, obtained from angular speed signals. The PDF labeled (D), corresponding to torque fluctuations, is obtained after removing the effect of stirrers inertia by deconvolution. The PDF labeled (C) corresponds to torque fluctuations after removing surface averaging from the time signal using a non-causal filter (see text). Note that the left-right asymmetry of curve (D) is reversed in (C).

the right side still remains. Being this the result of compensating a sort of time averaging, we expect an increase in the width of the PDF. In fact, this PDF is roughly five times wider than that for  $\tilde{\Omega}$ , as can be seen in the horizontal scale widening. It is worth to remark here that this is the primitive PDF from which an even more asymmetric PDF is obtained by averaging the underlying data. This does not contradict the Central Limit Theorem, because the conditions of that theorem are not met by these global magnitudes. Indeed, time filtering due to the inertia of the stirrer increases the correlation time of the angular speed fluctuations.

Now, if we compensate for surface averaging, we get not only wider PDFs but, in addition, a reversed left-right asymmetry, as displayed by curve labeled (C) in Fig. 4. This gives this PDF a shape reminiscent of that observed in the flow driven at constant angular speed, but much closer to a Gaussian. Remembering that power fluctuations can be ascribed to fluctuations of global torque when angular speed is held constant, it appears that stirrers with less ability in responding to flow changes makes normal stress fluctuations not only larger—as is certainly expected—, but also makes their statistics less Gaussian and even more asymmetric, a result which could be explained by the loss of local feedback from the flow to itself through the stirrer surface, due to the highly decreased response of the stirrer to flow stresses, imposed by the servo controller operating in the constant speed mode.

It is of interest to look at the time autocorrelation functions of fluctuations, displayed in Fig. 5a. The widest curve corresponds to the spectrum labeled 32 rps in Fig. 2, and the labels indicate the correspondence in the other two. It is clear that most of the correlation time for fluc-

tuations in the angular speed comes from the stirrer inertia. When this is removed by means of deconvolution, the autocorrelation time decreases by a factor 22, as shown by curve (D), and by removing the surface averaging it is decreased further by a factor 2.8 (curve C). Thus, torque fluctuations with inertia and averaging effects removed display a flat spectrum spanning four decades, and an autocorrelation time on the order of four milliseconds. We can interpret this number as an average time during which a flow structure at the global scale —characterized by some pattern in time— is acting on a stirrer. Interestingly, this time is the same found in a previous work<sup>13</sup> as the transit time of energy from the global scale to the smallest scales in a turbulent vortex in air, where the size of the volume occupied by the turbulent flow was similar to that in this experiment. This suggests that this measurement confirms, by using a method completely different, that the energy injected on the global scale of the flows quickly transits to the dissipative scale of the turbulent flow: in about 4 ms for the size of this experimental setup. This time appears too short to be the energy transfer time through the whole inertial range of the turbulent flow, and seems to contradict the idea of turbulence as being a cascade process. Thus, more work is required to confirm or disprove this assertion.

Finally, when cross correlations between upper and lower stirrers are calculated, we see that inertia filtering has a major role in increasing the cross correlation coefficient. This is displayed in Figure 5b by the wider curve, whose maximum is  $\chi_c \approx 0.75$ . Removing inertia gives the curve labeled (D), with a maximum value of only  $\chi_c = 0.25$ . By removing the surface averaging we get the curve labeled (C), showing a cross correlation coefficient of only  $\chi_c = 0.1$ . This can be understood by considering that inertia filtering and surface averaging have the effect of partially removing uncorrelated noise coming from the main flow turbulence, which has the effect of decreasing the cross-correlation coefficient. Of course, not vanishing cross correlation between stirrers is to be expected, due to torque transmission from one stirrer to the other through the fluid, but curves (D) and (C) show that turbulent flow fluctuations are strong enough to mask significantly the cross-correlation between stirrers.

#### IV. GLOBAL ROTATION STATISTICS

When we consider the sum of equations (2), what we get is a Langevin equation for fluctuations of the global shear,  $\tilde{\Omega}_1(t) + \tilde{\Omega}_2(t)$ , so to speak. As we have seen, this magnitude displays an extreme statistics. If we take instead the difference between equations (2), we get also a Langevin equation, but this time governing the global rotation of the flow. Let us denote by  $\Omega_R(t) = \Omega_1(t) - \Omega_2(t)$  the instantaneous angular speed of the global rotation. The PSD of  $\Omega_R(t)$  is displayed by the two bottom curves in Fig. 2, for stirrers rotating at 16 rps and 32 rps.

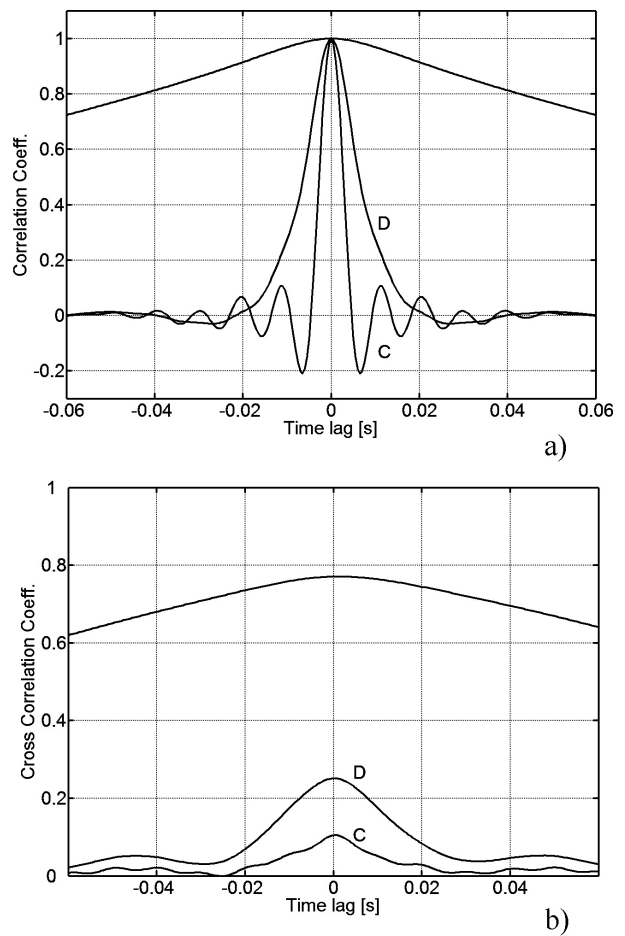


FIG. 5. a) Autocorrelation functions of signals corresponding to spectra in Fig. 2. The wider curve corresponds to the spectrum labeled 32 rps in fig. 2. The other two correspond to deconvolved (D) and compensated (C) signals. Autocorrelations fall to 0.2 in  $2.43 \times 10^1$  s,  $1.12 \times 10^2$  s, and  $3.96 \times 10^3$  s, respectively. b) Cross correlation coefficients between upper and lower stirrers. The cross-correlation coefficient is strongly reduced, first by deconvolution (D) and then by compensation (C) of the signals (see text).

We see that the spectrum labeled GR32 is essentially a straight line below 2.6 Hz, with a scaling of the form  $1/f^\alpha$  in that region. Thus, below this frequency this flow performs a global rotation that fluctuate in a self-similar manner around the mean global angular speed. This average angular speed should be strictly zero when the torques applied by the stirrers are precisely opposed. Above 2.6 Hz, the spectrum falls with an increasingly steeper slope, which indicates that global rotation is essentially a low frequency phenomenon, belonging to the global scale of the flow. The slope of the PSD of global rotation is slightly negative, as we can see in the plot. It turns out that its value seems to be remarkably close to  $-e^{-1}$ : in fact, the straight line in Fig. 2 has exactly this slope (see Appendix C). Note that the spectrum for stirrers rotating at 16 rps shares the same features, except for

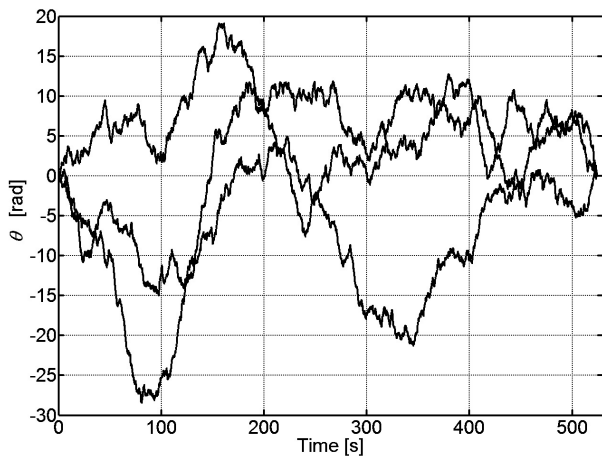


FIG. 6. Examples of sample-paths, corresponding to the integral of three samples of the global rotation angular speed. As they begin and finish at the same value (zero in this case), these paths are known as bridges.

the shift of its cutoff corner to a lower frequency. Thus, we have a Gaussian process characterized by a function  $\Omega_R(t)$  having a PSD which, in the relevant frequency interval, scales as  $f^{-1/e}$ . Given that we are dealing with an angular speed, it is natural to look at the flow global angle, which we define as

$$\theta(t) = \int_0^t \Omega_R(\zeta) d\zeta \approx \theta(t_k) = \sum_{i=0}^k \Omega_R(t_i) \Delta t, \quad (4)$$

were  $t_i = i\Delta t$  is the discretized time, and  $\Delta t$  is the time interval between sample points, for  $0 \leq t \leq T$  and  $0 \leq k \leq N$ . In our experiment, we took samples consisting of  $N = 2^{20}$  points in a time  $T \approx 524$  s. We used an oversampling factor  $\beta \approx 4$ , which makes the approximation made in (4) good enough. For each one of these samples, equation (4) defines a *sample-path*, in the language of Brownian motion theory. Given that the mean value of  $\Omega_R(t)$  is zero, these paths are in fact *bridges*<sup>14,15</sup>: they begin and finish at the same value; in this case, at  $\theta = 0$ . Fig. 6 displays three examples of these bridges.

The next question we can ask is: what is the scaling of the variance of the increments of these paths? The response that we found from our data is

$$\langle [\theta(t + \Delta t) - \theta(t)]^2 \rangle = C \Delta t^{\mu/2}, \quad (5)$$

where  $C$  is a constant and  $\mu \approx 2.7$  (see Appendix C). Being this a Gaussian process, the scaling (5) for the variance of time increments implies that Kolmogorov time structure functions must have the following scaling:

$$\langle |\theta(s) - \theta(t)|^n \rangle = C_n (s - t)^{n\mu/4}, \quad (6)$$

with  $s > t$ . Fig. 7 displays the left hand side of equation (6), obtained from the experimental data, and straight lines corresponding to the r.h.s., for  $n = 2, \dots, 7$  and

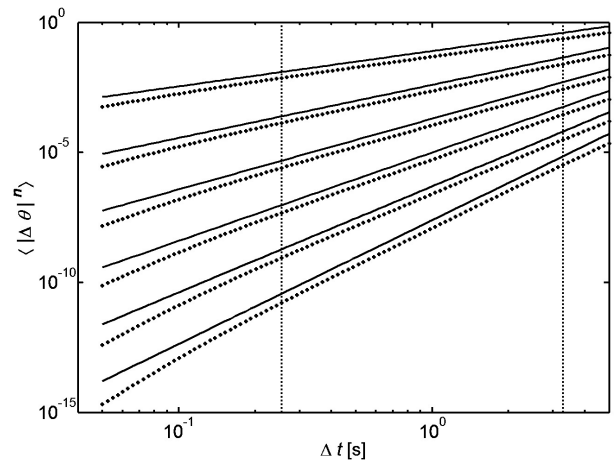


FIG. 7. Dots represent Kolmogorov time structure functions calculated from the experimental data. The straight lines have slopes corresponding to the exponent of time increments in equation (6). Fits of exponents were performed in the region between the vertical lines. From top to bottom,  $n = 2, \dots, 7$ . (see text)

$\mu = e$ . For clarity, the straight lines in the figure were raised just above the dots, and the vertical separation of structure functions was increased. In reality, all these curves have intersections in points in a neighborhood of  $(2.95, 0.2)$ . It can be seen that slopes of the straight lines appear to match properly the slopes of the straight portion of the experimental points in an interval spanning approximately one decade in the time increments between 0.2 s and 3.3 s. Thus, the global rotation exhibits a behavior compatible with an anomalous diffusion, specifically a superdiffusion<sup>16</sup> following scaling laws where the number  $e$  seems to play a preponderant role.

## V. CONCLUDING REMARKS

Most of the observed extreme statistics in fluctuations of global magnitudes in von Kármán swirling flows that we report here appears to be related to the dynamics of the stirring devices, or to the averaging of normal stresses on the vertical surface of vanes. Interestingly, the extreme statistics observed at constant rotation speed<sup>3</sup> seems to be linked to a rather extreme driving mode: the one corresponding to stirrers having nearly infinite inertia. In addition to the increase in the asymmetry of the PDF, the constant speed mode should increase the rms amplitude of torque fluctuations. This last conclusion is also given in a work in which this system was modeled by means of a stochastic Langevin equation<sup>17</sup>. Another interesting observation is that, once inertia and surface averaging are removed, it is found that torque fluctuations seem to behave like a white noise, having an almost Gaussian statistics<sup>18</sup>, a small autocorrelation time, and a flat spectrum. Given that in the experi-

ments by Titon and Cadot<sup>12</sup> water was used as working fluid, our conjecture to explain the difference between their almost symmetric rotation rate PDFs, as compared with those obtained in air when the flow is driven with stirrers rotating at constant torque, is that such difference is related to the huge ratio ( $\sim 10^3$ ) between the densities of water and air. In air, even using our light stirrers, inertia has a central role in the rotation dynamics. On the contrary, normal stresses exerted by water at similar Reynolds numbers will be roughly a hundred times larger. Thus, a stirrer driven at constant torque will be far more easily forced to follow the fluctuations in time of the space-averaged rotation of water near its surface. Additionally, this means that a servo motor will have a hard time attempting to keep a constant rotation rate in water if its power is similar to that used in experiments performed in air. Perhaps our most remarkable observation is the contrast between the statistics of global rotation versus global power injection (or global shear): when the driving device is allowed to respond to forces arising from the flow motion, the injected power fluctuations display a highly asymmetric PDF, having a right side with a stretched exponential shape, whereas global rotation fluctuations, derived from the same magnitudes, namely the stirrers angular speed fluctuations, have a perfectly Gaussian PDF. This last process is found to be a realization of a superdiffusion<sup>16</sup> by the motion of the turbulent flow at the global scale level. In the scaling laws of this anomalous diffusion the number  $e$  seems to appear in both, the exponent of the spectrum, and the exponents of the time structure functions. Our first rough estimation of the exponent on the low frequency section of the global rotation spectrum resulted in a number  $\alpha \approx -0.37$ , and we readily realized its closeness to  $-1/e$ . The existence of the number  $1/e$  in the solution of a well known problem in finance and probability theory, the so called secretary, marriage, best choice, or optimal stopping problem<sup>19,20</sup>, suggested us that  $-1/e$  could indeed be involved in the scaling exponents of the global rotation spectrum. Similarly, the scaling exponent in the variance of increments of the global angle  $\theta(t)$  resulted in a number close to  $e/2$ . The analysis depicted in Appendix C gives, in our view, a reasonable support to our conjectures.

On the one hand, we find indeed remarkable that the dynamics of global rotation in this turbulent flow, a system that we can properly classify as being *complex*, could be described by a far more simple 1D superdiffusion: an anomalous version of a 1D Brownian motion. On the other hand, distributions following power laws are always of interest in a number of fields in science, and finding power laws having irrational exponents in a natural phenomenon would be, in our view, fascinating. Even more if the number  $e$  is involved. Of course, this precludes any attempt of experimental verification, and first principles arguments will be necessary to prove our claim. Nevertheless, we finish the Appendix C with the result of a numerical calculation using a synthetic signal, giving

what we think is some additional support to our conjecture. From a practical point of view, and leaving aside the possible values that exponents could have, we believe that these results can be of interest as tests for models used in numerical simulation of confined turbulent flows.

## ACKNOWLEDGMENTS

We gratefully acknowledge S. Fauve, L. Vergara and I. Ispolatov for critical reading of the manuscript and suggestions. R.L. is indebted to G. Bobadilla, S. Navarro and G. Palma, whose support made possible this work as part of a sabbatical year project, and to P. Umbanhowar for highlighting, a long time ago, the advantages of pancake servomotors. Financial support for this work was provided by FONDECYT under grants #1090686 and #1040291.

## Appendix A: Materials and methods

The experimental setup used here is similar to that used in previous works<sup>3,4</sup>, except by the size. The diameter of the stirrers is  $D = 36$  cm and their separation is  $H = 47$  cm. The disks and their 8 vanes were cut from an expanded polystyrene plate of thickness  $T = 1.5$  cm and density  $\rho = 0.02$  g cm<sup>-3</sup>. They were assembled and covered with a thin layer of polyvinyl acetate glue, to increase their stiffness. Reinforcements made of thin aluminium disks of thickness  $t = 0.05$  cm and diameter  $d = 15$  cm were added in the central zone. These assemblies were directly coupled to Kollmorgen Servodisk® model JR16M4CH, low inertia, pancake type servomotors. The resulting moment of inertia of each stirrer, comprising polystyrene disk and vanes; motor armature; shaft; iron and aluminium coupling and reinforcing parts; and bolts was  $J = 2.0 \times 10^{-3}$  kg m<sup>2</sup>. In comparison, a stirrer having the same size but made of three-layer plywood of 6 mm thickness and driven by a 1 kW DC motor having an iron-core armature, would have a moment of inertia  $J = 5 \times 10^{-2}$  kg m<sup>2</sup>, which is about 25 times larger than that of the stirrers used in this experiment. The stirrers were driven by two Kollmorgen pulse width modulated (PWM) servo amplifiers type KXA-175, used in torque mode, meaning that in this case they operate merely as voltage-controlled current sources. Stirrers angular speeds  $\Omega_i$  were measured by means of frequency to voltage converters, using the pulses delivered by two Kollmorgen BA25I optical encoders attached to the shafts of the electric motors. These encoders give 1000 pulses per turn, and two of the output channels, A and B, are in phase quadrature. By using custom circuitry, transitions instead levels were detected, thus obtaining a resolution of 4000 pulses per revolution in the angular speed measurement system. All physical quantities were linearly mapped to voltages in the 0 to 10 V range. Specifically, the absolute stirrer rotation rate can vary between 0 and

60 rps. This range was mapped to the interval  $[0, 10]$  V. The absolute values of torque delivered by the DC motors vary from 0 to 3.72 N m, which was also mapped to the  $[0, 10]$  V interval. The experiment control was performed by a personal computer running programs under the National Instruments LabView platform. Electric signals were low-pass filtered using a IOtech Filter488/8 eight channel, 8th order elliptic low-pass filter, programmed through a National Instruments AT-GPIB/TNT (P&P) board, and digitized by a National Instruments AT-MIO-16X multifunction board. Data were acquired at 2 kS/s sampling rate using a cutoff frequency of 250 Hz. This oversampling level allows an excellent representation of signals up to the highest frequency passed by the filter, and leaves room for further numerical filtering of data. Whenever possible, appropriate offsets and gains were applied to the signals to take maximum advantage of the 16 bit digitizing card resolution.

## Appendix B: Data reduction and analysis

Appropriate level of shielding was used for signal cabling, but some hum from the power grid at 50 Hz and multiples is always present. This can be seen in some of the spectra drawn in Fig. 1 (e.g. the spectrum labeled 32 rps). Also, some peaks at several other frequencies, related to vibrations at the disks rotation frequencies and multiples, which can be ascribed to stirrers unbalancing, and angular vibrations related to motors electrical asymmetry, and so on, are also present. In all, our data allows for a maximum spectral frequency of 1 kHz, but no relevant signal components exist beyond 100 Hz. To clean up signals, we implemented a number of filters in the Fourier domain. All the spectral components beyond 120 Hz were zapped-out by using a low-pass, zero-phase filter having a sigmoidal shape, 0 dB gain in the band  $[0, 100]$  Hz and a higher than 350 dB attenuation for  $f > 120$  Hz. The frequency response for this filter is given by

$$H_N(f) = \frac{1}{2} \{1 - \tanh[\beta(|f| - f_c)]\}, \quad (\text{B1})$$

where  $\beta$  is a steepness factor. In our case,  $\beta = 0.1$ . Grid hum components were removed with zero-phase, Lorentzian-like band-stop filters tuned at 50 Hz and 100 Hz. These filters have the following frequency response:

$$H_{\text{hum}}(f) = 1 - \frac{g_n \zeta}{(|f| - f_0)^\nu + \zeta}, \quad (\text{B2})$$

and the parameters  $g_n$ ,  $\zeta$  and  $\nu$  were adjusted to match the shape of the hum peaks. Peaks related to vibrations and electrical asymmetries have their physical origin in the system dynamics. Causal filters are appropriate in this case, and we found that *LRC*-like notch or band-pass filters work fine to remove these peaks. Their transfer function (in the Laplace domain) is

$$G(s) = \frac{s^2 + (k/\tau)s + \omega_0^2}{s^2 + (1/\tau)s + \omega_0^2}, \quad (\text{B3})$$

Here,  $\omega_0$  and  $\tau$  are the center frequency and relaxation time, respectively, whereas  $k$  defines the filter as band-pass ( $k > 1$ ) or band-stop ( $0 < k < 1$ ). The band gain (attenuation) is determined by the value of  $k$ .

Filtering is also appropriate to deconvolve inertia filtering in torque fluctuations. Given that the stirrers are governed by a first order ordinary differential equation, the dynamical effect on the torque signal is simply that of a first order low-pass filter, having a transfer function

$$G_J(s) = \frac{1}{\tau s + 1}, \quad (\text{B4})$$

where  $\tau$  is the relaxation time. Its value is calculated from equation 3, which gives

$$\tau = \frac{J}{\gamma_M + 2\eta_F \bar{\Omega}}, \quad (\text{B5})$$

where  $J$  is the moment of inertia of the stirrer,  $\eta_F$  is the coefficient for the mean torque exerted by the flow on the stirrer,  $\bar{\Omega}$  is the mean value of the angular speed, and  $\gamma_M$  is a coefficient for electrical losses in the motors. Deconvolution in the Fourier domain is achieved simply by dividing the angular speed signal by  $G_J(i\omega)$  in the Fourier domain.

A remark is in order here. At constant torque drive mode, the drag torque signal obtained by deconvolution is not necessarily equivalent to the torque signal obtained when measurements are performed with stirrers rotating at constant angular speed. As we already pointed out, this case ideally corresponds to stirrers having infinite inertia. Thus, in this case there is no angular acceleration of the stirrer in response to normal stresses on the vertical surfaces of the vanes, which implies that there is no local feedback on the flow from one place to another in the neighborhood of the stirrer surface. As a consequence, we should expect some differences in the flow dynamics, which should explain why by deconvolving the signal we do not get the same PDFs as those obtained at constant angular speed.

## Appendix C: Estimates of the scaling exponents

It is known that determining exponents of power law distributions by standard methods is likely to produce biased estimates<sup>21–23</sup>. This is especially true when absolute values of exponents in power laws are larger than one. In our case, we have a spectrum with a power law scaling spanning two decades with an exponent  $\alpha \approx -0.37$ , and a power law scaling for the variance of the increments with an exponent  $\zeta \approx 1.4$ , which appears to be valid in a little more than one decade of time increments. To support our statement about the values of these exponents, namely  $\alpha = 1/e$  and  $\zeta = e/2$ , we estimated independently the values of the parameters  $\sigma$  and  $\mu$  in exponents written as  $\alpha = -1/\sigma$  and  $\zeta = \mu/2$ . Given that  $|\alpha| < 0.5$ , the PSD values span something less than one decade within the



TABLE I. Values of  $\mu$  extracted from the structure functions exponents

n	$\mu$	Linear scale fit	$\mu$	Log scale fit
		95% confidence bounds		95% confidence bounds
2	2.7180	2.7160 , 2.7200	2.7140	2.7100 , 2.7200
3	2.7013	2.6987 , 2.7040	2.7173	2.7133 , 2.7227
4	2.7050	2.7020 , 2.7070	2.7210	2.7160 , 2.7260
5	2.7048	2.7024 , 2.7072	2.7240	2.7200 , 2.7288
6	2.7040	2.7020 , 2.7053	2.7273	2.7227 , 2.7320
7	2.7383	2.7366 , 2.7394	2.7303	2.7263 , 2.7349

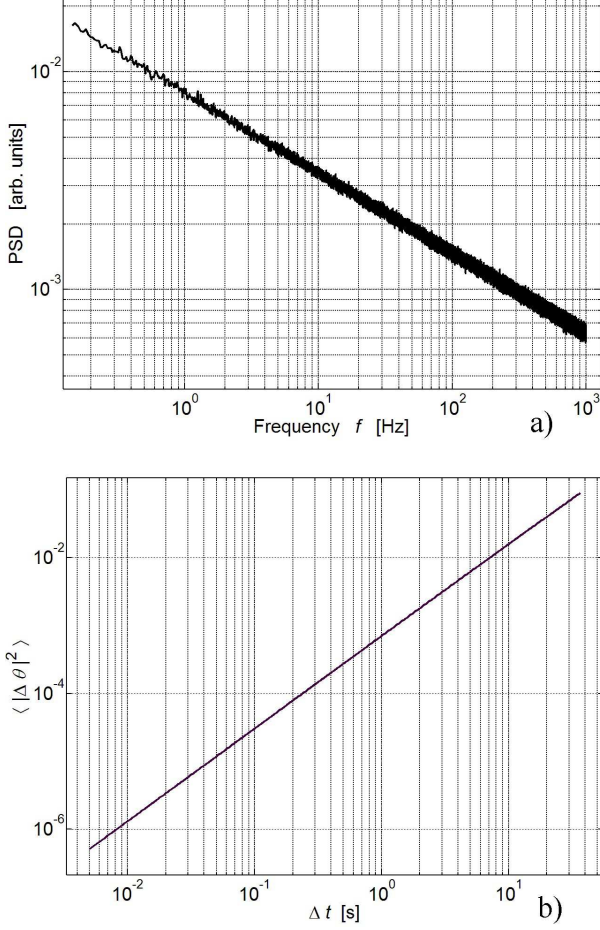


FIG. 8. a) Spectrum of a synthetic signal with scaling exponent  $-1/\alpha$ , with  $\alpha = 2.7187 \dots$ . b) The corresponding  $2^{\text{nd}}$  order structure function, with scaling exponent  $\mu/2$ , and  $\mu = 2.7198 \dots$ .

frequency range where the power law is valid. Then, using least squares fits in both, logarithmic and linear scales makes sense. We perform these fits in the frequency interval from  $7.6 \times 10^{-3}$  Hz to 2 Hz, which contains 262 spectrum points. From the logarithmic fit we obtain

$$\sigma = 2.728, \quad (\text{C1})$$

with  $R^2 = 0.931$  and 95% confidence bounds (2.640, 2.823). These bounds are  $-2.8\%$  and  $+3.8\%$  apart

from the value of  $e$ .

Performing a fit using

$$S = A f^{-1/\sigma}, \quad (\text{C2})$$

where  $S$  is the PSD, we obtain

$$\sigma = 2.702, \quad (\text{C3})$$

with  $R^2 = 0.97$  and 95% confidence bounds (2.661, 2.744). In both cases, the number  $e$  is roughly centered between the bounds, and we remark that in the last fit they are only  $\pm 2.1\%$  apart from the value of  $e$ . Each one of these two fits is consistent with the other, and both are consistent with the value  $e$  for the parameter  $\sigma$ . In fact, the estimate in (C1) is  $0.36\%$  greater than  $e$ , whereas in (C3) it is  $0.6\%$  smaller.

Now we consider the structure functions exponents. The scaling exponents are given by

$$\zeta_n = \frac{n\mu}{4}, \quad n = 2, 3, \dots \quad (\text{C4})$$

and we can proceed by fitting the curves to the data for each  $n$ , and from each exponent we can find values for  $\mu$ , using both linear and logarithmic scale fits. Our findings are summarized in Table I. We see that the values of  $\mu$  in Table I do not differ too much from  $e$ . At the very least, we have two coincident digits in all of the cases, but coincidences of three and even four digits are obtained in certain cases. We see a slight increasing trend in the logarithmic scale fits which does not seem to appear in the linear scale fits.

To conclude this analysis, we give here the result of a numerical calculation using a synthetic signal  $s_j$ ,  $j = 1, 2, \dots$ , consisting of 40 samples, each one having  $N = 2^{22}$  points, giving a total of  $M \approx 1.7 \times 10^8$  sample points, and having a spectrum that scales as  $f^{-1/\sigma}$ , with  $\sigma = 2.7187 \dots$ , which is close enough to  $e$ . The spectrum is plotted in Fig. 8 a). The  $2^{\text{nd}}$  order structure function is displayed in Fig. 8 b). It scales as  $\Delta t^{\mu/2}$ , with  $\mu = 2.7198 \dots$ . Although the agreement is reasonably good, this of course does not prove our conjecture. But this result is at least consistent with the role that we think  $e$  could play in the scaling exponents.

- 
- \* Also at *Grupo de Ciencias de la Tierra y del Espacio* (GCTE).
- <sup>1</sup> G. Falkovich and K.R. Sreenivasan, “Lessons from hydrodynamic turbulence.” *Phys. Today* **59**, 43 (2006).
  - <sup>2</sup> J.L. Lumley and A.M. Yaglom, “A century of turbulence.” *Flow, Turbulence and Combustion* **66**, 241 (2001).
  - <sup>3</sup> R. Labbé, J.-F. Pinton and S.Fauve, “Power fluctuations in turbulent swirling flows.” *J. Phys. II France* **6**, 1099 (1996).
  - <sup>4</sup> J.-F. Pinton, P.C.W. Holdsworth and R. Labbé, “Power fluctuations in a close turbulent shear flow.” *Phys. Rev. E* **60**, R2452 (1999).
  - <sup>5</sup> S.T. Bramwell, P.C.W. Holdsworth and J.-F. Pinton, “Universality of rare fluctuations in turbulence and critical phenomena.” *Nature* **396**, 552 (1998).
  - <sup>6</sup> S.T. Bramwell, K. Christensen, J.-Y. Fortin, P.C.W. Holdsworth, H.J. Jensen, S. Lise, J.M. López, M. Nicodemi, J.-F. Pinton and M. Sellitto, “Universal fluctuations in correlated systems.” *Phys. Rev. Lett.* **84**, 3744 (2000).
  - <sup>7</sup> T. Antal, G. Droz, G. Györgyi and Z. Rácz, “ $1/f$  Noise and extreme statistics.” *Phys. Rev. Lett.* **87**, 240601 (2001).
  - <sup>8</sup> T. Antal, G. Droz, G. Györgyi and Z. Rácz, “Roughness distributions for  $1/f^\alpha$  signals.” *Phys. Rev. E* **65**, 046140 (2002).
  - <sup>9</sup> G. Palma, T. Meyer and R. Labbé, “Finite size scaling in the two-dimensional XY model and generalized universality.” *Phys. Rev. E* **66**, 0261089 (2002).
  - <sup>10</sup> G. Mack, G. Palma and L. Vergara, “Corrections to universal fluctuations in correlated systems: The two-dimensional XY model.” *Phys. Rev. E* **72**, 026119 (2005).
  - <sup>11</sup> G. Palma, “Temperature dependence of universal fluctuations in the two-dimensional harmonic XY model.” *Phys. Rev. E* **73**, 046130 (2006).
  - <sup>12</sup> J.H. Titon and O. Cadot. “The statistics of power injected in a closed turbulent flow: Constant torque versus constant velocity forcing.” *Phys. Fluids* **15**, 625 (2003).
  - <sup>13</sup> R. Labbé, C. Baudet and G. Bustamente, “Experimental evidence of accelerated energy transfer in turbulence.” *Phys. Rev. E* **75**, 016308 (2007).
  - <sup>14</sup> L.C.G. Rogers and D. Williams. *Diffusions, Markov processes and martingales*. Second edition. Vol. 1. Cambridge University Press. Cambridge, UK (2003).
  - <sup>15</sup> D. Revuz and M. Yor. *Continuous martingales and Brownian motion*. Third edition. Springer-Verlag. Berlin, Heidelberg; Germany (1999).
  - <sup>16</sup> P. Siegle, I. Goychuk and P. Hänggi, “Origin of Hyperdiffusion in generalized Brownian motion.” *Phys. Rev. Lett.* **105**, 100602 (2010).
  - <sup>17</sup> N. Leprovost, L. Marié and B. Dubrulle, “A stochastic model of torques in von Kármán swirling flow.” *Eur. Phys. J. B* **39**, 121 (2004).
  - <sup>18</sup> In fact, the abrupt cutoff in the spectrum (C) in Fig. 2 is likely to be at the origin of the asymmetry in the PDF of the compensated signal. This problem is unavoidable because in practice it is impossible to increase without limit the signal to noise ratio, which is what finally establishes the usable measurement bandwidth.
  - <sup>19</sup> R.P. Freeman, “The secretary problem and its extensions: a review.” *Int. Stat. Rev.* **51**, 189 (1983).
  - <sup>20</sup> F.T. Buss, “A unified approach to a class of best choice problems with an unknown number of options.” *The Annals of Probability* **12**, 882 (1984).
  - <sup>21</sup> A. Clauset, C. R. Shalizi and M. E. J. Newman, “Power-law distributions in empirical data.” *SIAM Rev.* **51**, 661 (2009).
  - <sup>22</sup> E. P. White, B. J. Enquist and J. L. Green, “On estimating the exponents of power-law frequency distributions.” *Ecology* **89**, 905 (2008).
  - <sup>23</sup> M. E. J. Newman, Power laws, Pareto distributions and Zipf’s law. *Contemp. Phys.* **46**, 323 (2005).